Crystallization of $Fe_{73.5}Cu_1Nb_3Si_{13.5}B_9$ structure and kinetics examined by X-ray diffraction and Mossbauer effect spectroscopy

1992 J. Phys.: Condens. Matter 4 3195

(http://iopscience.iop.org/0953-8984/4/12/013)

J. Phys.: Condens. Matter 4 (1992) 3195–3214. Printed in the UK

Crystallization of $Fe_{73.5}Cu_1Nb_3Si_{13.5}B_9$: structure and kinetics examined by x-ray diffraction and Mössbauer effect spectroscopy†

G Hampel, A Pundt and J Hesse

Institut für Metallphysik und Nukleare Festkörperphysik, Technische Universität, Mendelssohnstrasse 3, 3300 Braunschweig, Federal Republic of Germany

Received 15 August 1991, in final form 4 November 1991

Abstract. Changes in the structure of the amorphous alloy $Fe_{73.5}Cu_1Nb_3Si_{13.5}B_9$ were investigated after annealing for 1 h in a temperature range from 450–800 °C using x-ray diffraction scattering and Mössbauer effect spectroscopy. Between 520 and 550 °C nanocrystalline $Fe_{80}Si_{20}$ grains with the DO_3 structure (diameter of about 10 nm) are embedded in an amorphous grain boundary phase. Above 650 °C the grain size increases and the amorphous grain boundary phase disappears. The Fe–B phases form and a new paramagnetic phase is observed. Furthermore the kinetics of the amorphous-to-nanocrystalline phase transition of this alloy was examined by x-ray diffraction observing the development of crystallization with time at a fixed annealing temperature of 520 °C. The beginning of crystallization appears at times less than 2 min, most grains developing in the first 10 to 20 min while after about 5 min the grain size remains constant with a diameter of about 10 nm.

1. Introduction

Nanocrystalline alloys with the composition $Fe_{74.5-x}Cu_xNb_3Si_{22.5-y}B_y$, called 'finemet' [2], are an object of investigation due to their particular magnetic properties [2–5]. In particular the alloy with the composition $x = 1$ and $y = 9$ shows very soft magnetic properties with coercitivities H_c of the order of 0.01 A cm^{-1} and initial permeabilities μ_i of the order of 10^5 after annealing from the amorphous phase for 1 h in the temperature range 480–550 °C [4]. These properties are only comparable with those of Co-based amorphous alloys and permalloys. The soft magnetic properties are related to a magneto-crystalline anisotropy averaging out, to a low or vanishing magnetostriction and to a nanocrystalline structure with very small grains of about 10 nm in diameter obtained through the annealing procedure [5, 6]. Increasing the annealing temperature by about 100 °C produces much bigger grain sizes of about 100 nm (microcrystalline structure) connected with an increase in coercitivity by three orders of magnitude and a decrease in the initial permeability [4].

These features give rise to the investigation of the physical reasons for the properties of the alloy system $Fe_{74.5-x}Cu_xNb_3Si_{22.5-y}B_y$ in more detail: for example the alloy with $x = 1$ and $y = 6$ was recently examined using Mössbauer effect spectroscopy (MS) and x-ray diffraction (XRD) in the amorphous state and after annealing

† Results first presented at the spring meeting of the German Physical Society 1991 [1].

0953-8984/92/123195+20$04.50

above 550 °C for 1 h by Zemčik *et al* [7] and Fujinami *et al* [8]. The effect of Cu on the structure and crystallization behaviour of this alloy with $y = 9$ and $x = 0, 0.5, 1, 1.5$ was examined by Kataoka *et al* [9] using XRD, MS, differential scannning calorimetry and differential thermal analysis in a temperature range 743–923 K. Hono *et al* [10] have investigated the microstructure of the alloy with $x = 1$ and $y = 9$ by atomic probe field ion microscopy and Kohmoto *et al* [11] examined the structure of this alloy using XRD and MS in the amorphous state and after annealing at 550 and 800 °C for 1 h.

Our results described here were first presented at the spring meeting of the German Physical Society 1991 [1] where Jiang *et al* [12] presented a similar contribution supporting our results.

We have analysed the structure of the alloy $Fe_{73.5}Cu_1Nb_3Si_{13.5}B_9$ in detail in the as-quenched amorphous state and after annealing at 450, 520, 550, 650 and 800 °C for an annealing time of 1 h using XRD and MS. In these investigations we tried to improve the results by combining XRD and MS and by fitting both kinds of spectra with suitable mathematic functions. Two additional phases were identified: an amorphous grain boundary phase for the nanocrystalline structure at 520 and 550 °C which contains the original amorphous phase at 520 °C and a paramagnetic phase which belongs to the microcrystalline structure at 800 °C.

Furthermore, we have examined the kinetics of crystallization of $Fe_{73.5}Cu_1Nb_3Si_{13.5}B_9$ by XRD observing the development of crystallization over time at an annealing temperature of 520 °C. Mössbauer spectra of this alloy annealed for different times at an annealing temperature of 520 °C were also collected and will be published in detail in [13].

2. Sample preparation and experimental details

Amorphous ribbons of $Fe_{73.5}Cu_1Nb_3Si_{13.5}B_9$ with a dimension of 15 mm in width and about 20 μm in thickness were produced by the melt-spinning technique at the Vacuumschmelze GmbH Hanau.

In order to determine the development of the changes in the structure of the partially crystallized samples the amorphous ribbons were annealed at temperatures T_A of 450, 520, 650 and 800 °C for 1 h under vacuum.

To examine the kinetics of the transformation into the nanocrystalline structure the ribbons were annealed in a salt solvent at a temperature of 520 °C for different times t_A = 2, 4, 8, 16, 32 and 60 min.

The amorphous and the crystalline state of the differently treated samples were characterized using XRD and MS. XRD measurements were performed in a Siemens Θ–2Θ diffractometer in reflection geometry using Mo Kα radiation ($\lambda = 0.71069$ Å [14]). The x-ray intensity was measured continuously as a function of the scattering angle 2Θ between 15° and 65°.

Mössbauer spectra were collected in transmission geometry using the natural content of the ^{57}Fe isotope in the samples. The γ-radiation was produced in a source containing 20 mCi of ^{57}Co in Rh matrix. Both x-ray and Mössbauer spectra were collected at room temperature.

3. Results

Before investigating the properties of $Fe_{73.5}Cu_1Nb_3Si_{13.5}B_9$ the quality of the as-

quenched alloy was examined using XRD and conversion electron Mössbauer spectroscopy (CEMS). XRD spectra collected from both sides of the as-quenched ribbons show identical shapes typical for the amorphous phase demonstrating the initial amorphous state of the as-quenched alloy. Details about the MS and CEMS spectra of the amorphous alloy will be published later [13].

First we present results obtained by XRD examination of the samples annealed for 1 h at different temperatures.

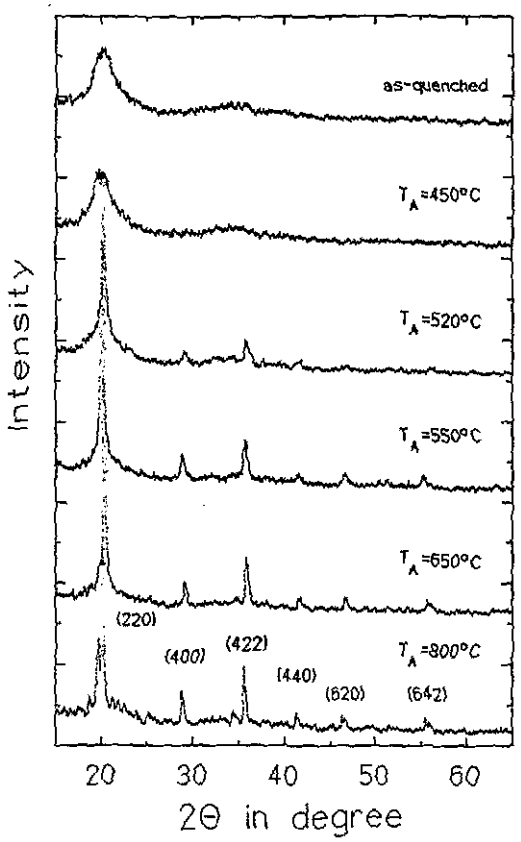

Figure 1. Series of Mo-Kα x-ray spectra of $Fe_{73.5}Cu_1Nb_3Si_{13.5}B_9$ at different annealing temperatures for an annealing time of 1 h. The dominant peak at about $2\Theta \approx 20$ °C is used for a quantitative evaluation. Its sharp peak is fitted using two Gaussian lines (figure 3). For $T_A = 800$ °C the dominant lines of the DO_3 structure of $Fe_{80}Si_{20}$ are indicated. For details see the text.

3.1. X-ray diffraction

3.1.1. The structure of $Fe_{73.5}Cu_1Nb_3Si_{13.5}B_9$. XRD patterns of the alloy in the as-quenched state and also after annealing at a temperature of 450 °C for 1 h show the typical first and second broad diffuse maximum characteristic for the short-range order of the amorphous state (figure 1). After annealing at $T_A = 520$ °C sharp lines appear resulting from the BCC structure of a crystalline α-FeSi phase. The intensity of these peaks increases with increasing temperature up to $T_A = 550$ °C. At $T_A = 650$ °C Fe–B phases start to form. At $T_A = 800$ °C some new small peaks appear revealing the formation of several new phases. In figure 2 the peaks shown could be indicated in the following way:

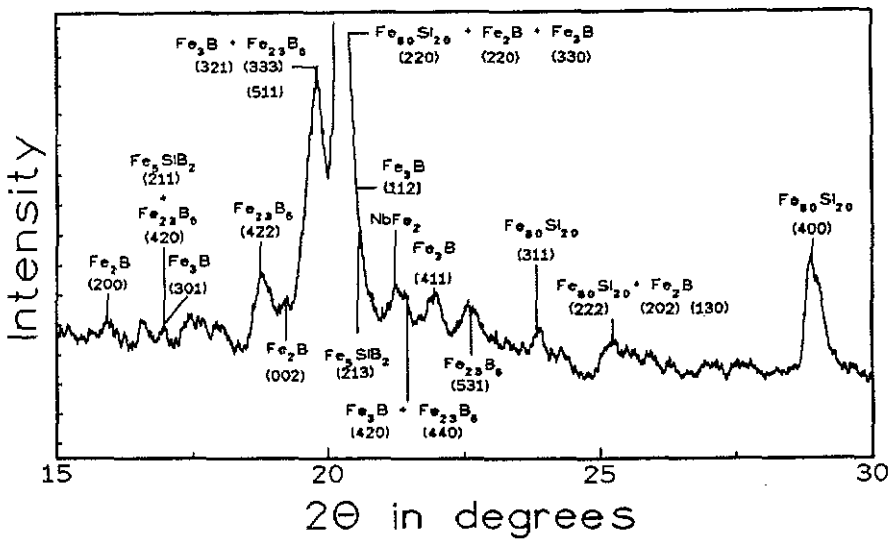

Figure 2. Indication of the peaks of the x-ray spectra of $Fe_{73.5}Cu_1Nb_3Si_{13.5}B_9$ annealed for 1 h at a temperature of 800 °C. The superstructure of the DO_3 structure of the $Fe_{80}Si_{20}$ grains are shown as well as the peaks of the Fe_2B, tetragonal Fe_3B and FCC $Fe_{23}B_6$. Probably some other phases comprising Fe and one or two other components of the original alloy may occur, for example tetragonal $NbFe_2$.

(i) A superstructure of the (222) and (311) peak of the α-Fe–Si phase shows the formation of an ordered Fe–Si phase with DO_3 structure (figure 12).

(ii) Some Fe–B phases are observed and can be related to BCT Fe_2B, tetragonal Fe_3B and FCC $Fe_{23}B_6$ (for references see table 1).

Probably some other phases comprising Fe and one or two other components of the original alloy may occur, for example a tetragonal $NbFe_2$ phase, a FeNbB phase (suggested by Jiang *et al* [12]) or a tetragonal Fe_5SiB_2 phase. In table 1 the lattice parameters for some known Fe intermetallic phases are listed. To identify the peaks one must take into consideration that the lattice parameters of the phases occurring in the examined alloy may deviate from the ideal values. It seems to be certain that neither orthorhombic FeB and Fe_3B phases, ϵ-FeSi, η-Fe_5Si_3 nor orthorhombic $FeSi_2$ phases occur.

For a detailed evaluation of the XRD spectra the first short-range order maximum of the amorphous state and the (220) peak of the DO_3 structure of crystalline Fe–Si were fitted by Gaussian lines (figure 3). However, with only one Gaussian line it is impossible to obtain a good fit to the (220) peak in the spectra from the alloys annealed at $T_A = 520$ and 550 °C. Here two Gaussian lines (a sharp high G_1 and a broad flat G_2 one) are needed for a good approximation of the XRD lineshape.

Gaussian lines were chosen to determine the position and width of the peaks and their relative fractions of the spectra. It is always possible to use Lorentzian lines for this approximation without significantly changing the results. This for example has been done by Jiang *et al* [12].

Figure 4 shows the fit parameters such as peak intensity of the maximum, half-width and position of the peak plotted against the annealing temperature. At $T_A =$ 520 °C a characteristic variation in the parameters according to the amorphous-to-nanocrystalline phase transition can be observed. While the peak intensity is constant

Table 1. Lattice parameters for several intermetallic Fe phases collected from the literature.

Phase	Structure	Lattice parameter Å			Ref.
		a	*b*	*c*	
α-Fe	BCC	2.8664	—	—	[25]
α'-Fe_3Si	DO_3	5.64	—	—	[25]
α'-Fe_3Si	DO_3	5.655	—	—	[17]
ϵ-FeSi	Cubic	4.46	—	—	[25]
ϵ-FeSi	Cubic	4.489	—	—	[17]
η-Fe_5Si_3	Hexagonal	6.757	—	9.440	[25]
η-Fe_5Si_3	Hexagonal	6.7552	—	4.7144	[17]
Fe_2Si	Cubic	2.81	—	—	[25]
$FeSi_2$	Orthorhombic	9.879	7.799	7.839	[25]
$FeSi_2$	Tetragonal	2.69	—	5.08	[25]
FeB	Orthorhombic	4.053	5.495	2.946	[25]
Fe_2B	TBC	5.099	—	4.240	[25]
Fe_2B	TBC	5.11	—	4.25	[26]
Fe_3B	Tetragonal	8.63	—	4.29	[27–29]
Fe_3B	Orthorhombic	5.433	6.656	4.454	[26, 30]
Fe_3B	Orthorhombic	5.43	6.66	4.45	[26, 28, 29]
$Fe_{23}B_6$	FCC	10.67	—	—	[26]
Fe_5SiB_2	Tetragonal	5.52	—	10.339	[25]
$NbFe_2$	Tetragonal	4.840	—	7.895	[31]

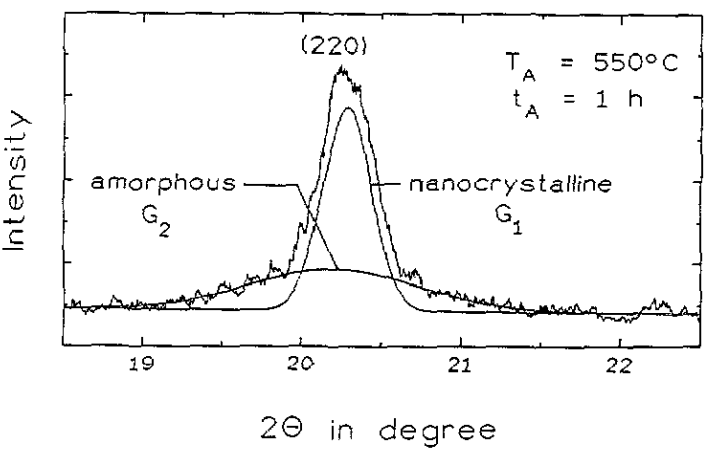

Figure 3. The dominant peak of figure 1 at about $2\Theta \approx 20$ °C is fitted using two Gaussian lines. One Gaussian line (the sharp one with high intensity, G_1) is assigned to the (220) peak of the Fe–Si DO_3 structure. The second (broad one with lower intensity, G_2) we relate to the amorphous grain boundary phase.

for the amorphous state it increases drastically at the transition temperature. The peak intensity of the second small and broad Gaussian line (G_2) at $T_A = 520$ °C and $T_A = 550$ °C remains of the same order of magnitude as those of the amorphous alloys. The half-width of the first Gaussian line (G_1) decreases by around 20% at the phase transition. The half-width of the second broad Gaussian line (G_2) lies between that of the amorphous and that of the nanocrystalline one. For $T_A \geqslant 520$ °C the

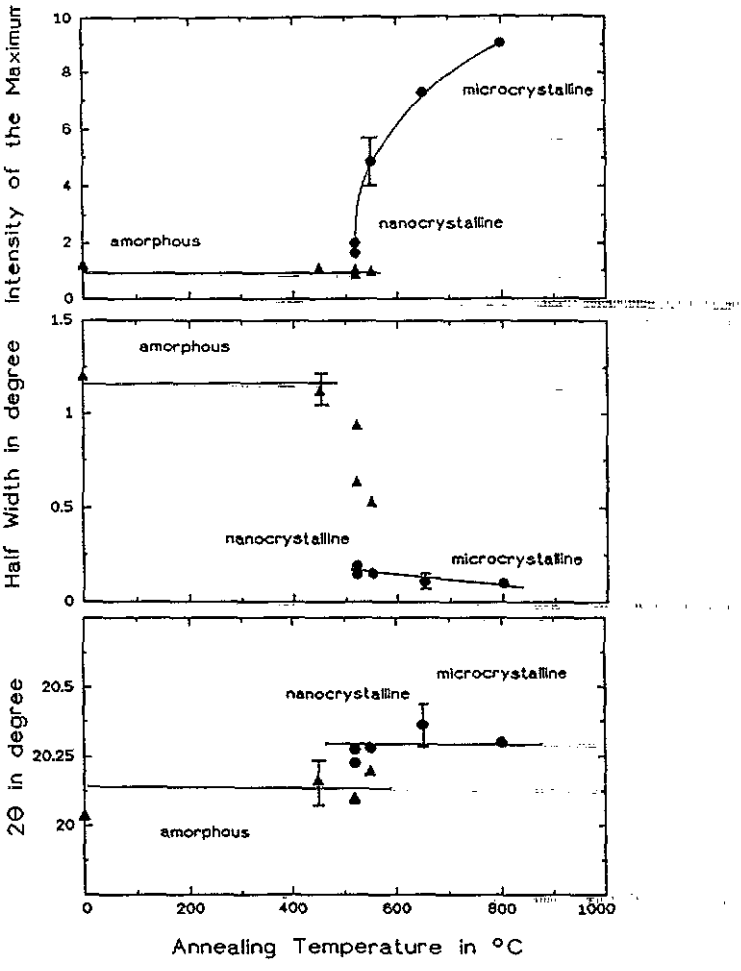

Figure 4. Temperature dependence of the fit parameters as intensity of the maximum, half-width and position of the line in degree to the XRD measurments presented in figure 1: ●, (220) peak of the Fe–Si DO_3 structure (line G_1 of the Gaussian fit (figure 3)); ▲, the first diffuse maximum of the amorphous phase respectively the amorphous grain boundary phase (line G_2 of the Gaussian fit (figure 3)). Between $T_A = 450$ °C and $T_A = 520$ °C the amorphous-to-nanocrystalline phase transition takes place. From the position of the diffraction peaks we determined the lattice parameter for the BCC cell of the DO_3 structure of the Fe–Si phase to 2.84(±0.01) Å remaining constant in the temperature range 520–800 °C and the distance of next-neighbour atoms for the amorphous grain boundary phase to about 2.5 Å remaining constant from room temperature (as-quenched state) up to 550 °C . For details see the text.

half-width of G_1 decreases with increasing T_A.

In the temperature range 520–800 °C the position of the (220) peak (G_1) is constant within an accuracy of about ±0.1°. The peak position of the amorphous state is also constant, but it is shifted by about 0.3° compared with the crystalline lines. The peak position of the second flat line G_2 at $T_A = 520$ °C and $T_A = 550$ °C lies on one line with those of the amorphous state within the error bars.

3.1.2. The kinetics of the phase transition in $Fe_{73.5}Cu_1Nb_3Si_{13.5}B_9$. Using XRD, studies of the kinetics of the amorphous-to-nanocrystalline phase transition are possible when observing the development from the broad diffuse maxima of the amorphous phase to sharp lines which develop after annealing the sample above the transition temperature and which increase with increasing annealing time t_A.

In figure 5 XRD spectra of the alloy $Fe_{73.5}Cu_1Nb_3Si_{13.5}B_9$ annealed at a temperature of $T_A = 520$ °C for annealing times t_A between 2 and 60 min are shown together with the spectrum of the alloy in the as-quenched state for comparison. Already at $t_A = 2$ min a small sharp line has grown from the first broad amorphous maximum in the spectrum. After $t_A = 4$ min the intensity of the sharp line has increased and some new lines have appeared corresponding to the BCC lines of the DO_3 structure of Fe–Si. Increasing the annealing time to 1 h results in an increase in the intensity of the sharp lines. Additionally more lines with higher diffraction index appear.

These spectra were analysed (like the T_A-dependent measurements) by fitting the dominant peak with two Gaussian lines, a sharp high G_1 and a broad flat G_2 one. In figure 6 the fit parameters are plotted against the annealing time. The intensity of the maxima of the sharp lines (G_1) increases most rapidly in the first 10 to 20 min. The half-width of the lines corresponding to the amorphous grain boundary (G_2) and the Fe–Si phase (G_1) is nearly constant after about 2 min up to 1 h of annealing. The position of the lines of the amorphous (G_2) and nanocrystalline (G_1) phase varies by only about 1%.

3.2. The Mössbauer spectra

Using MS different Fe–Si and Fe–B phases can be analysed by means of different hyperfine fields produced at the nuclei of ^{57}Fe atoms. The Mössbauer spectra of the alloy $Fe_{73.5}Cu_1Nb_3Si_{13.5}B_9$ in the as-quenched state and after annealing for 1 h at different temperatures are shown in figure 7. In the as-quenched state and after annealing at $T_A = 450$ °C six broad lines appear which is typical for the amorphous structure with a broad hyperfine field distribution. Both spectra show an asymmetry in the intensity of the lines referring to a distribution of isomer shifts. After annealing above 520 °C the spectra exhibit many sharp lines which can be fitted by using five subspectra each consisting of six lines (see section 4.2 and [13]).

4. Discussion

4.1. X-ray diffraction

4.1.1. The stucture of $Fe_{73.5}Cu_1Nb_3Si_{13.5}B_9$. The behaviour of the fit parameters for the broad flat line G_2 at $T_A = 520$ and 550 °C shown in figure 4 is similar to those of the amorphous alloys, while the sharp high line G_1 can be attached to a nanocrystalline FeSi phase. Thus in the temperature range 520–550 °C nanocrystalline Fe–Si grains are embedded in an amorphous rest phase, which separates the single Fe–Si grains. Therefore this amorphous rest phase is called the 'amorphous grain boundary phase' (Birringer *et al* [15]).

Using the Scherrer formula [16] the grain size in the alloys annealed above 520 °C can be determined by means of the half-width and line position (figure 8). For $T_A = 520$ and 550 °C the average grain size of the FeSi crystallites is determined to approximately 10 nm (±3 nm) in good agreement with studies by transmission

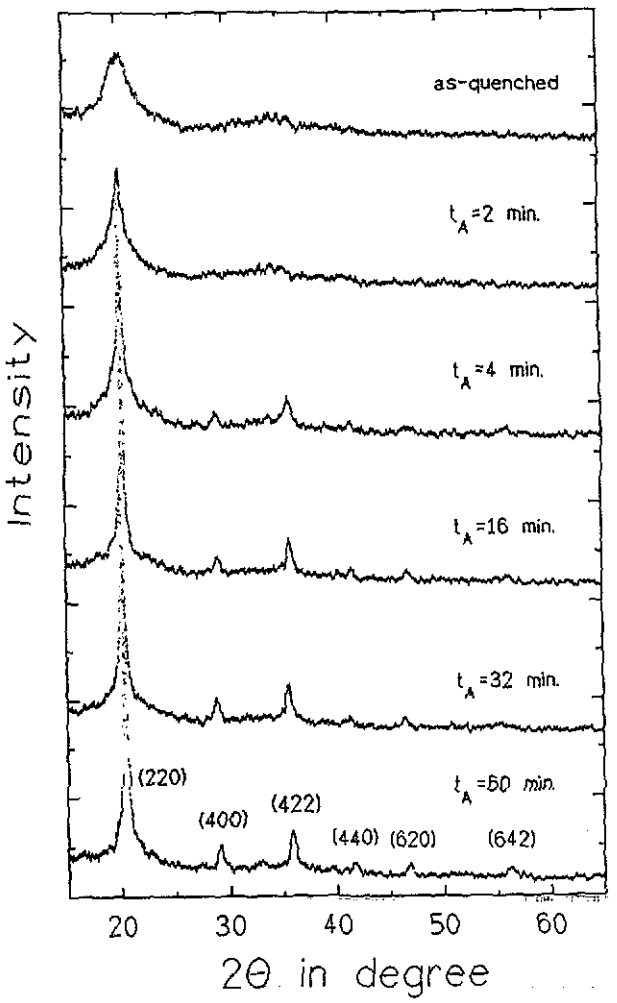

Figure 5. X-ray spectra of $Fe_{73.5}Cu_1Nb_3Si_{13.5}B_9$ for different annealing times at an annealing temperature of $T_A = 520$ °C (similar to the description given in figure 1). The dominant peak at $2\Theta \approx 20$ °C is assigned to the (220) peak of the DO_3 structure of $Fe_{80}Si_{20}$ and to the amorphous peak. This peak is fitted with two Gaussian lines (G_1 and G_2). For $t_A = 60$ min the dominant lines of the DO_3 structure of $Fe_{80}Si_{20}$ are indicated. For details see the text.

electron microscopy (TEM) [4]. With increasing temperature the mean grain size increases up to a diameter of about 30 nm at 800 °C. These values are approximately a factor 3–4 too small compared with the largest grains and about a factor 3 too large compared with the smallest grains as observed by TEM studies [4].

From the position of the lines in XRD the lattice parameter of the BCC cell of the DO_3 structure of Fe–Si is determined to be 2.84 (±0.01) Å remaining constant for the examined temperature range 520–800 °C and lying between the lattice parameter of BCC α-Fe (2.866 Å) [17] and the lattice parameter for the cubic cell of ordered α′-Fe_3Si (2.822 Å) [17] (table 1). A lattice parameter of 2.84 Å corresponds to a concentration of Si in the Fe–Si grains of about 19 to 20 at.% ($Fe_{80}Si_{20}$ i.e. a fraction Fe/Si ≈ 4) [18]. This is an indication of a large decomposition in the alloy during the amorphous-to-nanocrystalline phase transition because the as-quenched

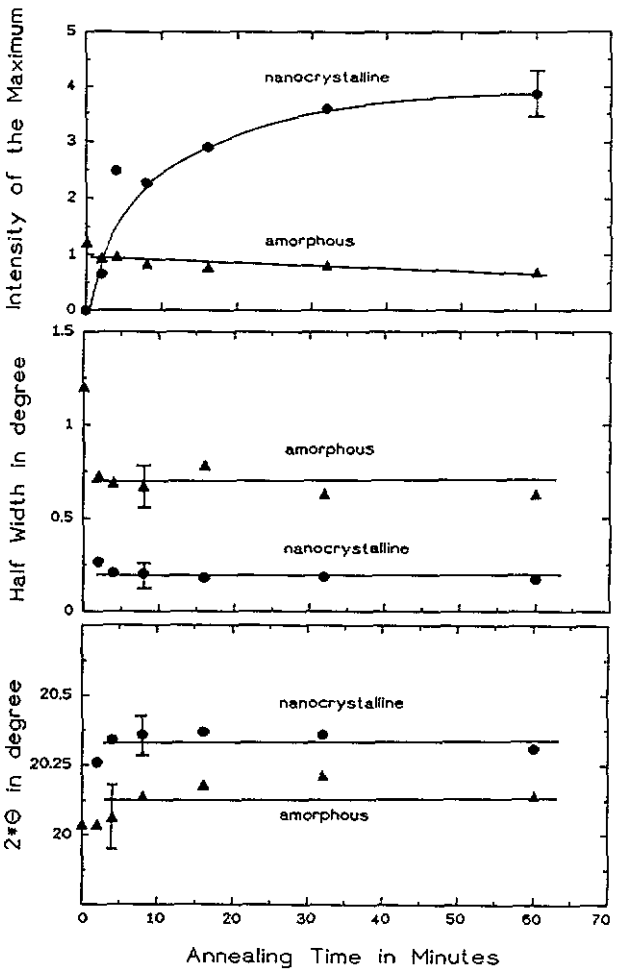

Figure 6. Time dependence of the fit parameters: intensity of the maximum, half width and position of the line to the XRD measurements presented in figure 3. ●, the (220) peak of the Fe–Si DO_3 structure (line G_1 of the Gaussian fit); ▲, the first diffuse maximum of the amorphous grain boundary phase (line G_2 of the Gaussian fit). The intensity of the (220) peak increases most in the first 10 to 20 min meaning that in this time most crystallites are formed. From the position of the diffraction peaks we determined the lattice parameter for the BCC cell of the DO_3 structure of the Fe–Si phase to 2.84(±0.01) Å and the distance of nearest-neighbour atoms for the amorphous grain boundary phase to be about 2.5 Å remaing constant for annealing times larger than 5 min.

alloy contains only 13.5 at%Si and 73.5 at%Fe (i.e. fraction Fe/Si $\approx$ 5.4). Besides, Cu and Nb are not soluble in α-Fe, Si or α-FeSi [19] and x-ray peaks of Fe–B phases cannot be observed above T_A = 650 °C (figures 1 and 2). Therefore the amorphous grain boundary phase consists of less Fe and Si and more B, Cu and Nb than the as-quenched amorphous phase.

The distance of nearest-neighbour atoms x_m for the as-quenched amorphous state and the amorphous grain boundary phase can be determined to be about 2.5 Å in the whole temperature range (where these phases occur) by using the following formula

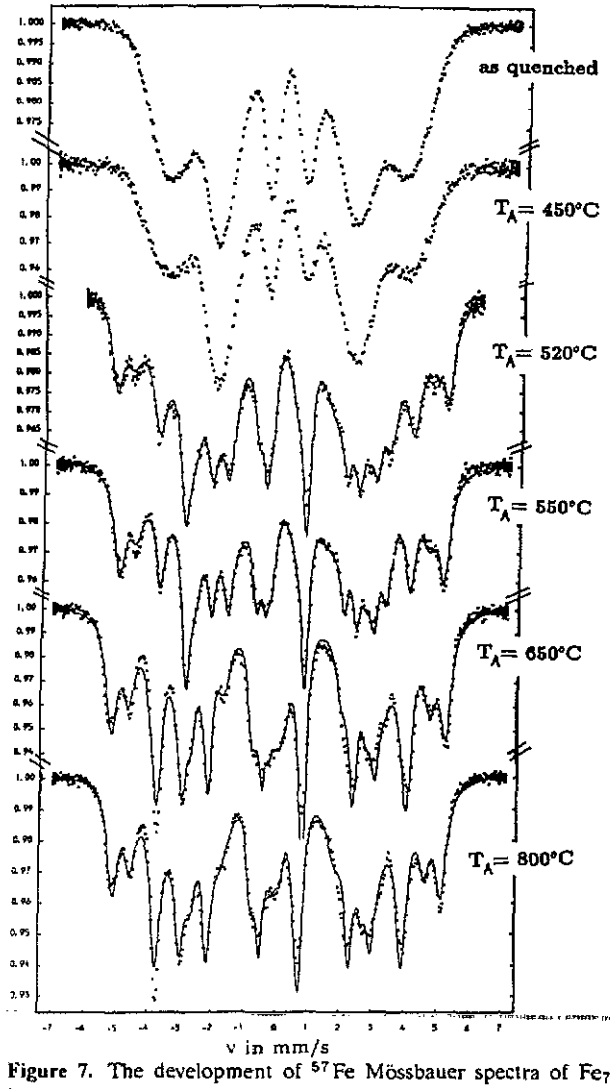

Figure 7. The development of ^{57}Fe Mössbauer spectra of $Fe_{73.5}Cu_1Nb_3Si_{13.5}B_9$ collected at room temperature for different annealing temperatures (as indicated in the figure) at an annealing time of 1 h. The spectra of the as-quenched alloy and of the alloy after annealing at $T_A = 450$ °C are typical for an amorphous structure. Above annealing at $T_A = 520$ °C the spectra exhibit in many lines which indicate that some new crystalline phases develop.

taken from Guinier [16]:

$$\frac{2 \sin \Theta_m}{\lambda} = \frac{1.23}{x_m}$$

where Θ_m denotes the angle of the first short-range order maximum and λ the wavelength of x-ray radiation.

4.1.2. The kinetics of the phase transition in $Fe_{73.5}Cu_1Nb_3Si_{13.5}B_9$. The discussion on the two Gaussian lines of the time-dependent spectra is carried out in a manner similar to that used for the temperature-dependent measurments: the higher sharp

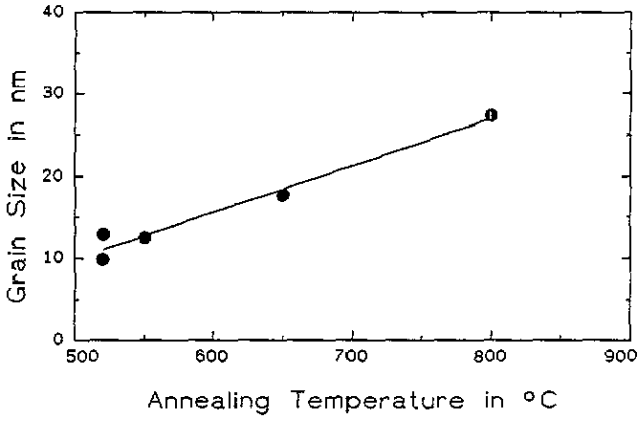

Figure 8. Dependence of the grain sizes of $Fe_{80}Si_{20}$ on the annealing temperature for an annealing time of 1 h. The grain size was determined from the width and position of the XRD lines using Scherrer's formula [16]. For details see the text.

line G_1 represents the nanocrystalline Fe–Si phase with DO_3 structure and the flat broad line G_2 represents the amorphous grain boundary phase.

From the position of the lines the lattice parameter of the BCC cell of the DO_3 structure of Fe–Si can be determined to be 2.84 (±0.01) Å remaining constant for t_A = 5–60 min. Therefore the concentration of Si in the Fe–Si grains is constant and amounts to 20 at.% ($Fe_{80}Si_{20}$) in this annealing time interval. The distance of nearest-neighbour atoms in the amorphous grain boundary is also constant and amounts to 2.5 Å.

Using the Scherrer formula the size of the $Fe_{80}Si_{20}$ grains was determined to be about 10 nm (±3 nm) for about t_A = 5–60 min. In the first 5 min the mean grain size increases from 6 to 10 nm with increasing annealing time assuming a linear dependence (figure 9).

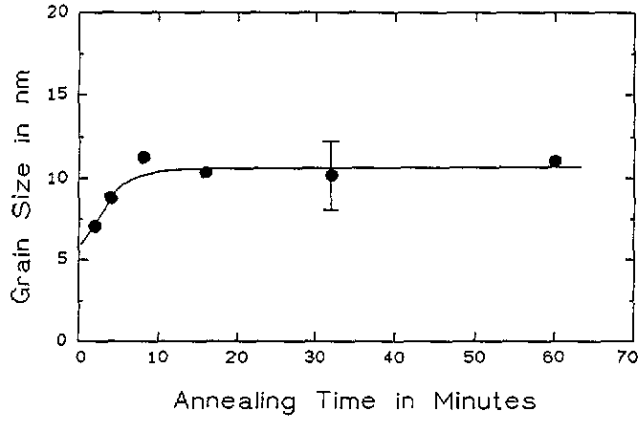

Figure 9. The grain sizes of $Fe_{80}Si_{20}$ against the annealing time for the annealing temperature of 520 °C as determined from the width and position of the XRD lines using Scherrer's formula [16]. In the first 5 min a linear increase of the grain sizes is observed. After this annealing time the grain sizes are constant during the rest of the examined time interval.

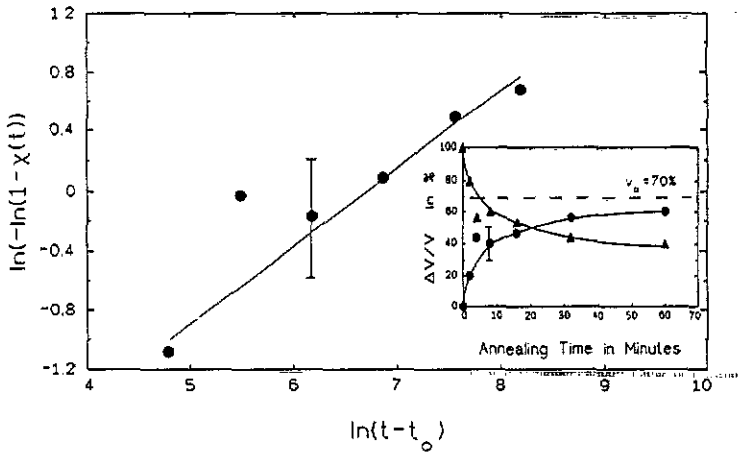

Figure 10. Avrami plot derived from data of XRD measurments; $\chi(t) = (v(t)/v_0) =$ fraction of the transformed nanocrystalline volume with respect to the total volume. Inset: Fractions of the untransformed amorphous and transformed nanocrystalline volumes for different annealing times at an annealing temperature of 520 °C. Both fractions approach a saturation, which amounts to 30% for the untransformed and 70% for the transformed volume.

The inset in figure 10 shows the relative fractions of the amorphous and nanocrystalline volume for different annealing times at $T_A = 520$ °C. They are determined from the area under the two Gaussian lines to within an accuracy of about 10%. The untransformed volume decreases with increasing annealing time approaching a minimum (of about 30%) after 1 h, while the transformed volume increases with increasing temperature approaching a saturation volume v_0 of about 70% after 1 h. For both volume fractions 70% of the saturation is obtained after about 10 min indicating that most of the nanocrystallites develop within this time. After $t_A = 60$ min about 90% of the saturation is reached, about 10% of the alloy is comprised of the original amorphous phase.

After reaching saturation all nanocrystalline $Fe_{80}Si_{20}$ grains are formed from the amorphous phase. Between the grains the amorphous grain boundary phase is developed with a different constitution from that of the as-quenched amorphous phase.

The nucleation rate and growth at the amorphous-to-crystalline transition for isothermal transformations with homogeneous and undisturbed growth are often interpreted in terms of the Johnson–Mehl–Avrami kinetics which describes the transformed crystalline volume $v(t)$ of the volume v_0† at an annealing time t from the beginning of the crystallization at a time t_0 [20, 21]:

$$\chi(t) := v(t)/v_0 = 1 - \exp(-f * (t - t_0)^n) \tag{1}$$

with

$$f = f_0 * \exp(-E_0/kT).$$

f denotes the frequency of nucleation rate and growth. n is the Avrami exponent which describes the kind (morphology) of nucleation (n_n) and growth (n_g): $n = n_n +$

† The volume v_0 is the whole volume which will be transformed into the new nanocrystalline phase.

n_g with $0 \leqslant n_n \leqslant 1$ and $1 \leqslant n_g \leqslant 3$. ($n_n = 1$ for steady state nucleation, $n_n = 0$ for athermal growth of quenched-in nuclei, $n_g = 1.5$ for primary growth, $n_g = 3$ for eutectic and polymorphous growth [21].) More values of n are summarized in Christian [20]. E_0 is the mean activation energy for crystallization. An Avrami plot, a plot of $\ln(-\ln(1-\chi(t)))$ against $\ln(t-t_0)$, should be a straight line with slope n and an intercept $\ln(\tau)$ with $\tau^n = 1/f$.

To examine what kind of law the nucleation and growth transformation of the investigated alloys is following we test the validity of the Johnson–Mehl–Avrami kinetics. Figure 10 shows a plot with $\chi(t)$ as the nanocrystalline volume normalized to the total volume v_0, which is the saturation volume of the nanocrystalline phase. This volume adapts to 70% of the whole volume of the sample. The beginning of the crystallization is approximated to $t_0 = 0$ because already after 2 min of annealing a new sharp line appears. From the Johnson–Mehl–Avrami plot in figure 10 the Avrami exponent n is determined within the error bars to be about 0.5 and f to be 0.03 Hz. Under the assumption that f_0 is equal to the Debye frequency of about 10^{13} Hz the mean activation energy is determined to be about 2.3 eV for nucleation. $n \approx 0.5$ is an unusual value for an Avrami exponent. In order to explain such a small value of n we have to consider different mechanisms superposing on each other during the crystallization of the glass $Fe_{73.5}Cu_1Nb_3Si_{13.5}B_9$:

(i) Following the proposal of Köster *et al* [22] only small additions of Cu atoms to the alloy leads to an increase in 'quenched-in' nucleation sites, which accelerates the nucleation of the primary crystallization. In the ideal case no energy is needed for nucleation (athermal nucleation) and n_n has to be zero.

(ii) This athermal nucleation is accompanied by thermal activated nucleation which yields to n_n between zero and one.

(iii) In our mind the growth of the crystallization nuclei is inhomogeneous because if in an amorphous alloy the local distribution of atoms fluctuates the growth of the nuclei is dependent on the local surrounding (homogeneous and undisturbed growth is assumed in equation (1)). Therefore values of $n_g < 1$ may occur and an evaluation other than the Johnson–Mehl–Avrami one may be possible for the observed phase transition.

On the one hand the addition of Nb atoms to the alloy retards the growth of the nuclei [22] because Nb inhibits the diffusion of the Si and B atoms [8]. Therefore the increase in the grain size is limited by a diameter of only about 10 nm. On the other hand the nucleation rate is facilitated by the addition of Cu atoms [22] which increases the number of 'quenched-in' atoms and prevents long diffusion.

4.2. Mössbauer spectra

The Mössbauer spectra are fitted with five subspectra each consisting of six lines (figure 11) [13]. Four subspectra ((*a*)–(*d*) in figure 11) correspond to different Fe sites which can occur in the ordered region of Fe–Si with a DO_3 structure for Si concentrations between 10 and 25 at.% [23]. Figure 12 shows the unit cell of the DO_3 structure of ordered Fe_3Si (for 25 at.% Si). The DO_3 structure consists of an A-lattice with A sites occupied by Fe atoms and a D-lattice with D sites occupied by Fe or Si atoms. All atoms on D sites have eight nearest-neighbour Fe atoms, while Fe atoms on A sites can have a varying number of nearest-neighbour Fe or Si atoms depending on the Si concentration . If a Fe atom on an A site has n nearest-neighbour Fe atoms, it is called an A_n site. The probability for the occurrence of different A_n

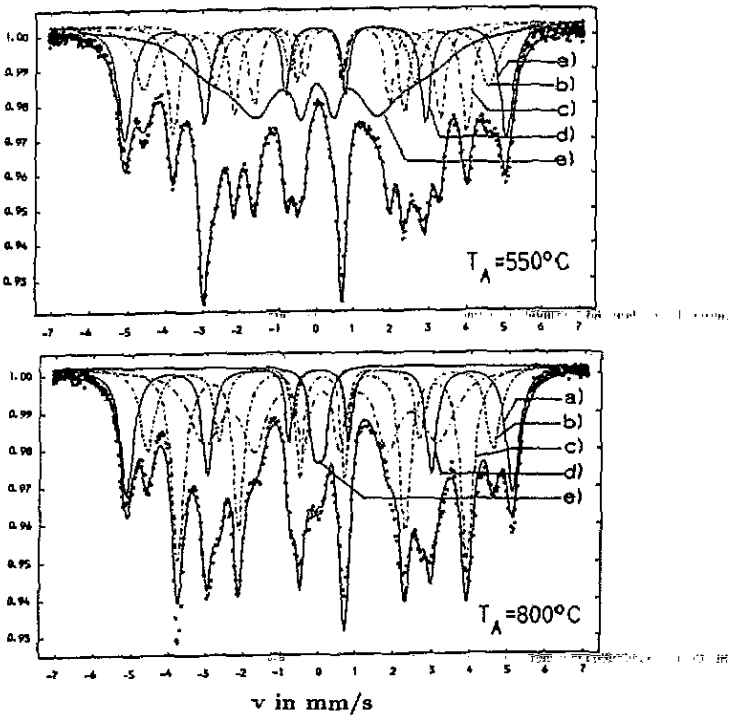

Figure 11. Mössbauer spectra of $Fe_{73.5}Cu_1Nb_3Si_{13.5}B_9$ and their decomposition into five subspectra each consisting of six lines. Four subspectra are related to Fe atoms on different sites of the Fe–Si DO_3 structure: (*a*) Fe atom on D site; (*b*) Fe atom on A_6 site; (*c*) Fe atom on A_5 site; (*d*) Fe atom on A_4 site. One subspectum (*e*) is related to the amorphous grain boundary phase at $T_A = 550$ °C respectively to the paramagnetic FeNb or FeNbB phase at $T_A = 650$ °C.

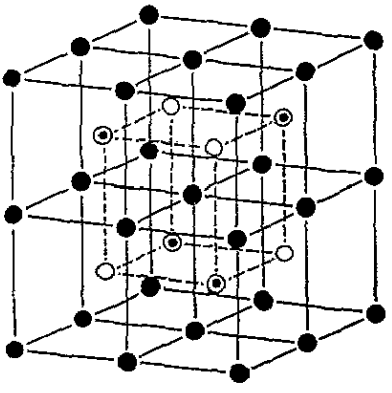

Figure 12. Unit cell of the DO_3 structure of Fe_3Si, which consists of an A-lattice (—) and a D-lattice (- - -): ●, Fe atom on A site; ⊙, Fe atom on D site; ○, Si atom on D site. For details see the text.

sites is dependent on the Si concentration [23]. For the alloy $Fe_{73.5}Cu_1Nb_3Si_{13.5}B_9$ annealed above 520 °C A_4, A_5, A_6 and D sites were found corresponding to the named four spectra. (Due to the fact of having the same mean hyperfine field A_7, A_8 and D sites cannot be distinguished using MS.) The fifth broad subspectrum can be

related to the amorphous grain boundary phase for annealing temperatures between 520 and 550 °C ((*e*) in figure 11). The amorphous grain boundary phase of the alloy annealed at 520 °C contains structures of the as-quenched amorphous phase in contrast to those annealed at 550 °C. Details of the fit of the Mössbauer spectra of the alloy annealed at 520 °C are described in [13]. For $T_A = 650$ °C the broad fifth spectrum disapears. On the other hand a new broad single line develops indicating a new phase with a Curie temperature below room temperature. Now this single line spectrum is described by the fifth spectrum.

The fit parameters for each spectrum are the mean hyperfine field $\bar{H}$, the isomer shift v_{iso}, the fraction of a single subspectrum consisting of six lines with respect to the whole spectrum and the broadening of the lines ΔH which occurs in amorphous alloys and is due to the broad hyperfine field distribution. For the alloy annealed at 520 °C one more fit parameter is used describing the fraction of the amorphous phase in the amorphous grain boundary phase which shows a structure similar to the as-quenched amorphous phase in the surrounding of a Fe atom.

The intensity ratios of the six lines of the subspectra are constant—3:2.5:1:1:2.5:3—for all fits. The temperature dependence of the fit parameters are shown in figures 13(*a*)–(*d*) and listed in table 2.

The mean hyperfine field is constant for A_4, A_5, A_6 and D sites over the temperature range 520–800 °C and agree well with the values of $\bar{H}$ for these sites published by Stearns [23] (tables 2 and 3, and figure 13(*a*)), while $\bar{H}$ from the fifth spectrum changes from about 200 to about 10 kG between 520 and 650 °C indicating that the amorphous grain boundary phase disappears in this temperature interval and a new paramagnetic phase, e.g. FeNb or FeNbB as suggested by Jiang *et al* [12], arises (figure 13(*a*)). The fraction of the amorphous grain boundary phase amounts to about 50% at $T_A = 520$ °C and 40% at $T_A = 550$ °C and the fraction of the paramagnetic phase amounts to about 5% between $T_A = 650$ and 800 °C (figure 13(*b*)). We estimate the error bars in this determination to be about ±5%. The fractions of the D, A_4 and A_6 sites show only a small temperature dependence, while the fraction of the A_5 sites increases by about 20% between $T_A = 550$ and 650 °C indicating the occurrence of a new phase which may be TBC Fe_2B, because the $\bar{H}$-fields of this alloy are of the same order of magnitude as the $\bar{H}$-fields occurring from Fe atoms on A_5 sites in ordered Fe–Si with about 20 at.% Si (table 3).

In addition the mean hyperfine field of Fe atoms on A_6 sites are of the same order of magnitude as the mean hyperfine field of tetragonal Fe_3B (table 3). Therefore it is difficult to separate the tetragonal Fe_3B phase using MS. Only the determination of the Si concentration in the Fe–Si grains (see later) indicates that the ratio of the subspectrum of the A_6 sites to the whole spectrum is too large. This is a hint for the presence of an Fe_3B phase in the alloy system $Fe_{73.5}Cu_1Nb_3Si_{13.5}B_9$ after annealing in the temperature range 520–800 °C. For details about the determination of the Fe_3B phase using MS see [13]. XRD measurements clearly show a TBC Fe_3B phase only at T_A=800 °C because at $T_A = 520$ and 550 °C the pattern of the amorphous grain boundary phase is superposed on the lines of Fe_3B.

The isomer shift v_{iso} is constant over the examined temperature range for all subspectra and agrees with the values published by Stearns [23] apart from the subspectrum from Fe atoms on A_4 sites.

The broadening of the lines ΔH for the fifth subspectrum decreases by nearly 100 kG from 550 to 650 °C indicating that the amorphous grain boundary phase disappears and a new crystalline phase arise at 650 °C. For the subspectra of A_4, A_5

Table 2. Fit-parameters of the Mössbauer effect spectra against the choosen annealing temperatures.

T_A Sites/subspectra	520	550	650	800
	$\bar{H}$ (kG)			
$D+A_7+A_8$	316	316	321	319
A_6	286	285	290	286
A_5	244	243	241	238
A_4	195	195	194	192
Amorphous grain boundary phase	194	171	—	—
Paramagnetic phase	—	—	16	11
	Fractions of one subspectrum with respect to the whole spectrum (%)			
$D+A_7+A_8$	12.1	18.7	22.5	20.7
A_6	12.0	14.2	14.3	15.0
A_5	14.5	14.8	36.2	30.3
A_4	12.4	13.5	19.2	29.8
Amorphous grain boundary phase	49.0	38.8	—	—
Paramagnetic phase	—	—	7.8	4.3
	ΔH (kG)			
$D+A_7+A_8$	13.38	14.53	14.80	13.48
A_6	30.05	24.30	15.08	15.93
A_5	15.17	10.12	15.40	12.57
A_4	17.15	11.08	30.28	53.33
Amorphous grain boundary phase	106.5	121.0	—	
Paramagnetic phase	—	—	14.74	3.114
	v_{iso} (mm s^{-1})			
$D+A_7+A_8$	−0.037	−0.029	−0.026	−0.022
A_6	−0.007	−0.008	−0.002	−0.004
A_5	−0.099	0.092	0.061	0.063
A_4	0.175	0.163	0.140	0.045
Amorphous grain boundary phase	−0.029	0.001	—	—
Paramagnetic phase	—	—	−0.011	−0.032

and D sites ΔH is equal or smaller than 30 kG and shows no significant temperature dependence. Only for the A_4 sites does ΔH increase with increasing temperature up to about 50 kG at 800 °C (table 2 and figure 13(*d*)). Besides the fraction of the subspectrum of the A_4 sites to the whole spectrum increases a little from 520 to 800 °C and v_{iso} decreases for Fe atoms on A_4 sites (table 2 and figures 13(*b*)–(*d*)). We interpret this as a hint that a further phase has developed whose $\bar{H}$-field is similar to those of Fe atoms on A_4 sites, for example Fe_5SiB_2 (see tables 2 and 3). The increase in ΔH with increasing temperature rules out that this is the result of dynamical influences on the shape of the Mssbauer spectra, which is observed on other nanocrystalline systems such as Fe oxides [24].

From the fraction of D to A_4 sites the Si concentration can be determined to be about 20 at.% in good agreement with x-ray measurments. For this determination the probabilities of the appearance of D and A_4 sites in dependence on the Si

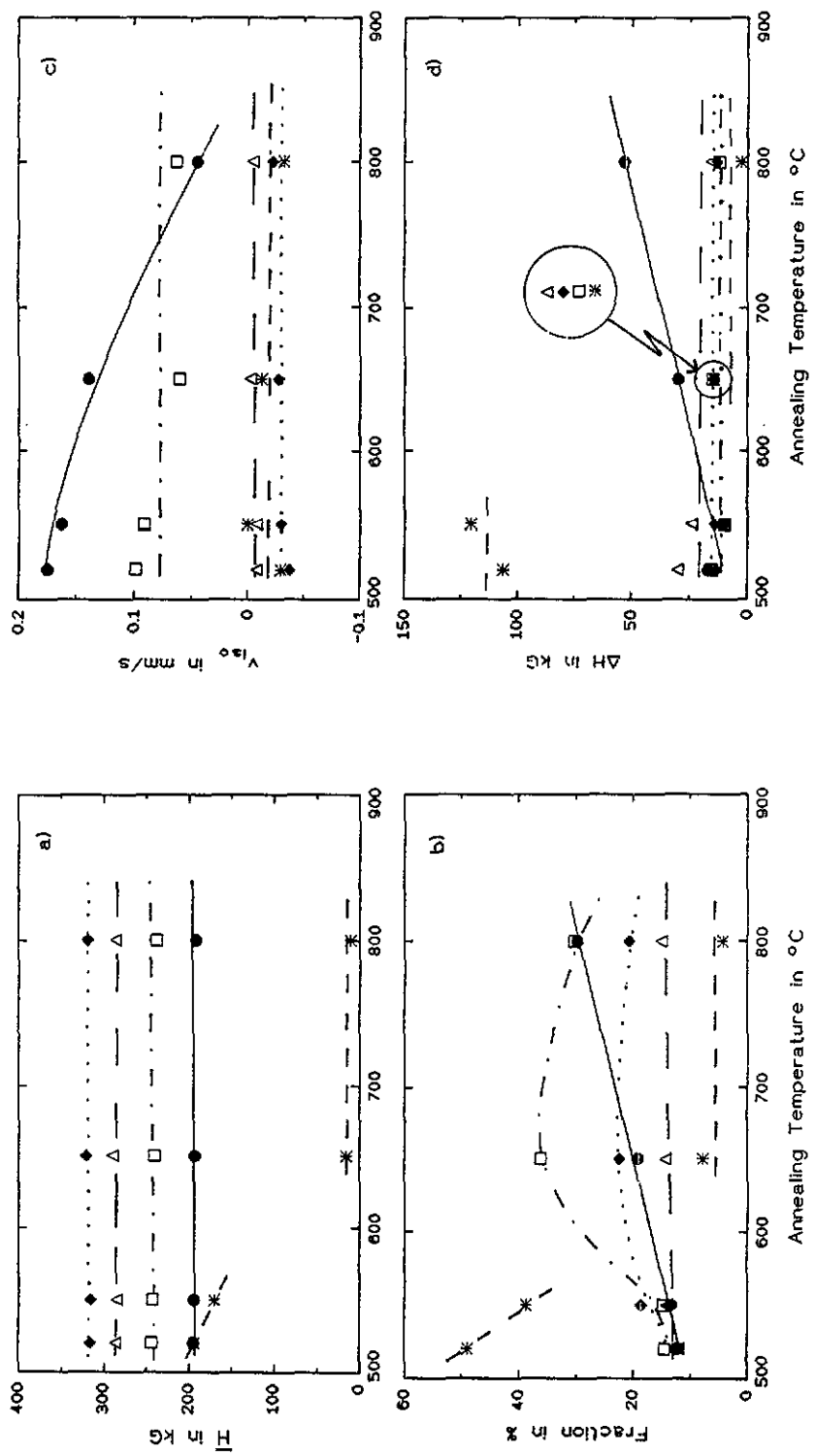

Figure 13. Dependence of the MS fit parameters on the annealing temperature: (*a*) mean hyperfine field $\bar{H}$; (*b*) the fraction of one subspectrum (six lines) to the whole spectrum; (*c*) isomer shift v_{iso}; and (*d*) the broadening of the lines ΔH on the annealing temperature. The values of the different subspectra are marked in the following way: A_4 sites, ● and ——; A_5 sites, □ and — · —; A_6, △ and — — —; D sites, ◆ and ·····, the fifth subspectrum (indicating the amorphous grain boundary phase at $T_A = 520$ and 550 °C and a new paramagnetic phase at $T_A = 650$ and 800 °C), * and - - -. The values are also given in table 2. For details see the text.

Table 3. Mean hyperfine field of several intermetallic Fe-phases collected from the literature.

Phase	Structure	$\bar{H}$ (kG)	$(\bar{H}/\bar{H}_{Fe})^a$	Ref.
α-Fe	BCC	330	1	
α′-Fe_3Si	DO_3 ($c_{Si} \leqslant 22\%$)			[23]
	D+A_8+A_7	308–323	0.934–0.978 ± 0.002	
	A_6	287 ± 1	0.871 ± 0.004	
	A_5	244 ± 1	0.738 ± 0.004	
	A_4	193 ± 1	0.585 ± 0.004	
	A_3 ($c_{Si} \geqslant 26\%$)	145 ± 3	0.44 ± 0.01	
FeB	Orthorhombic	117	0.354	[32, 33]
FeB	Orthorhombic	118	0.358	[30, 34]
Fe_2B	Tetragonal	240	0.727	[30, 33]
Fe_2B	Tetragonal	237	0.718	[34]
Fe_3B	Tetragonal	287 ± 2	0.861 ± 0.006	[35]
		225 ± 2	0.861 ± 0.006	
		260 ± 3	0.802 ± 0.006	
Fe_3B	Orthorhombic	236 ± 6	0.716 ± 0.02	[32, 36]
		260 ± 6	0.79 ± 0.02	
Fe_3B	Orthorhombic	235 ± 5	0.712 ± 0.02	[30]
		264 ± 5	0.8 ± 0.02	
Fe_5SiB_2	Tetragonal	170	0.515	[34]
		198	0.6	
		230	0.697	

[a] If possible $\bar{H}_{Fe}$ is taken from the respective indicated reference, otherwise a value of 330 kG is taken.

concentration published by Stearns [23] are used for reference. The small increase in the fraction of A_4 sites with increasing temperature indicates a small increase in the Si concentration of about 2% in the Fe–Si grains. Nevertheless the inaccuracy of the determination of the Si concentration using MS lies in this order of magnitude.

5. Conclusion

The results presented in this paper can be summerized as follows.

(i) The changes in structure of the alloy $Fe_{73.5}Cu_1Nb_3Si_{13.5}B_9$ have been investigated by XRD and MS, annealing the samples at different temperatures T_A for 1 h. Between $T_A = 450$ and 520 °C the amorphous-to-nanocrystalline phase transition is observed. At $T_A = 520$ and 550 °C nanocrystalline $Fe_{80}Si_{20}$ grains with diameters of about 10 nm are embedded in an amorphous grain boundary phase. The lattice parameter $a_{BCC} = 2.84$ Å of the DO_3 structure of ordered $Fe_{80}Si_{20}$ and the ratio of D to A_4 sites from the fit of the Mössbauer spectra give a concentration of Si of about 20 at.% in the Fe–Si grains. The fraction of the amorphous grain boundary phase determined by MS decreases from about 50% at $T_A = 520$ °C to about 40% at $T_A = 550$ °C. Decreasing the annealing temperature up to $T_A = 650$ °C a second phase transition takes place, the alloy becomes microcrystalline, the amorphous grain boundary phase has disappeared, Fe–B phases develop, whose fractions increase up to $T_A = 800$ °C, and a new paramagnetic phase with a mean hyperfine field of about 5 kG is observed by MS.

(ii) The kinetics of the phase transition of the alloy $Fe_{73.5}Cu_1Nb_3Si_{13.5}B_9$ has been investigated by XRD, annealing the samples at different times t_A at a temperature of 520 °C. The measurements show that the beginning of crystallization appears at times less than 2 min. After an increase in the grain size up to about 10 nm in the first 5 min the grain size remains constant up to 60 min of annealing time. Most crystallites develop during the first 10 to 20 min of annealing. The lattice parameter a_{BCC} of the DO_3 structure of the Fe–Si grains is constant and about 2.84 Å from $t_A = 5$ min up to $t_A = 60$ min, e.g. the Si concentration remains constant and about 20 at.% in the Fe–Si grains in this annealing time interval. The Avrami exponent $n = 0.5$ indicates that the amorphous-to-nanocrystalline phase transition is determined by nucleation and less by nucleation growth.

Acknowledgments

The authors wish to thank Dr H R Hilzinger and Dr G Herzer from the Vacuumschmelze GmbH Hanau for the amorphous alloy samples, as well Professor H Neuhäuser and Mr G Mathiak for the investigations performed on the samples using electron microscopy and the Deutsche Forschungsgemeinschaft for financial support.

References

[1] Hampel G, Pundt A and Hesse J 1991 *Verhandlungen der Deutschen Physikalischen Gesellschaft* (VI) **26** 1286
[2] Yoshizawa Y, Oguma S and Yamauchi K 1988 *J. Appl. Phys.* **64** 6044–6
[3] Herzer G 1989 *IEEE Trans. Magn.* **25** 3327–9
[4] Herzer G 1990 *IEEE Trans. Magn.* **25** 1397–402
[5] Hilzinger H R 1990 *Mater. Sci. Forum* **62–4** 515–20
[6] Herzer G 1991 *Mater. Sci. Engrg* A **133** 1–5
[7] Zemčík T, Jirásková Y, Závěta K, Eckert D, Schneider J, Mattern N and Hesske D 1991 *Mater. Lett.* **10** 313
[8] Fujinami M, Hashiguchi Y and Yamamoto T 1990 *Japan. J. Appl. Phys.* **29** L477–80
[9] Kataoka N, Inoue A, Masumoto T, Yoshihito J and Yamauchi K 1989 *Japan. J. Appl. Phys.* **28** L1820–3
[10] Hono K, Inoue A and Sakurai T 1991 *Appl. Phys. Lett.* **58** 2180
[11] Kohmoto O, Haneda K and Choh T 1990 *Japan. J. Appl. Phys.* **29** L1460–2
[12] Jiang J, Aubertin F, Gonser U and Hilzinger H R 1991 *Verhandlungen der Deutschen Physikalischen Gesellschaft* (VI) **26** 1286
[13] Pundt A, Hampel G and Hesse J 1992 Mössbauer effect studies on amorphous and nanocrystalline $Fe_{73.5}Cu_1Nb_3Si_{13.5}B_9$ *Z. Phys. B: Condens. Matter* at press
[14] Sagel K 1958 *Tabellen zur Röntgenstrukturanalyse* (Berlin: Springer)
[15] Birringer R, Herr U and Gleiter H 1986 *Suppl. Transactions of the Japan Institute of Metals, Grain Boundary and Related Phenomena, Proc. JIMIS* **4** 43–52
[16] Guinier A 1963 *X-Ray Diffraction in Crystals, Imperfect Crystals and Amorphous Bodies* (San Francisco, CA: W H Freeman) pp 72–143
[17] Pearson W B 1964 *A Handbook of Lattice Spacings and Structures of Metals and Alloys* (Oxford: Pergamon)
[18] Yelsukov Ye P, Barinov V A and Konygin G N 1986 *Phys. Met. Metall.* **62** 1136–44
[19] Hansen M 1958 *Constitution of Binary Alloys* (New York: McGraw-Hill)
[20] Christian J W 1970 *Physical Metallurgy* ed R W Chan (Amsterdam: North-Holland) p 471
[21] Scott M G 1983 *Amorphous Metallic Alloys* ed F E Luborsky (London: Butterworths) p 144
[22] Köster U, Schünemann U and Blank-Bewersdorff M 1991 *Mater. Sci. Eng.* A **133** 611–15
[23] Stearns M B 1963 *Phys. Rev.* **129** 1136–44

[24] Jing J, Zhao F, Yang X and Gonser U 1990 Magnetic relaxation in nanocrystalline iron-oxides *Hyperfine Interact.* **54** 571–6
[25] ICPDS 1981 *Metals and Alloys Data Book*
[26] Herold U and Köster U 1978 *Z. Metallkde.* **69** 326
[27] Walter J L, Bartram F and Russell R R 1978 *Metall. Trans.* A **9** 803
[28] Inal O T, Robino C V, Keller L, Yost F G and Karnowsky M M 1981 *J. Mater. Sci.* **16** 3183–93
[29] Takahashi M, Koshimura M and AbuzukaT 1981 *Japan. J. Appl. Phys.* **20** 1821–32
[30] Choo W K and Kaplow R 1977 *Metall. Trans.* A **8** 417
[31] Shiga M and Nakamura Y 1987 *J. Phys. Soc. Japan* **56** 4040–6
[32] Chien C L 1977 *Phys. Rev.* B **18** 1003–15
[33] Murphy K A and Hershkowitz N 1973 *Phys. Rev.* B **7** 23–31
[34] Hang Nam Ok and Morrish A H 1980 *Phys. Rev.* B **22** 3471–80
[35] Le Caer G and Dubois J M 1981 *Phys. Status Solidi* a **64** 275–62
[36] Budnik J I, Sanchez F H, Zhang Y D, Choi M, Hines W A, Zhang Z Y, Ge S H and Hasegawa R 1987 *IEEE Trans. Magn.* **23** 1937–44